Tribology International 214 (2026) 111368

Contents lists available at ScienceDirect

Tribology International

journal homepage: www.elsevier.com/locate/triboint

Understanding fretting fatigue in dovetail joints: Slip accumulation, stick-slip evolution, joint angle and crack initiation

Qiqi Xiao [a], Can Wang [a], Yuxuan Wu [a], Gang Chen [b], Lihua Wang [c,*], Magd Abdel Wahab [a,c,d,**]

[a] Soete Laboratory, Department of Electrical energy, metals, mechanical constructions and systems, Faculty of Engineering and Architecture, Ghent University, Belgium
[b] School of Chemical Engineering and Technology, Tianjin University, Tianjin 300072, China
[c] School of Aerospace Engineering and Applied Mechanics, Tongji University, Shanghai 200092, China
[d] Parallel and Distributed Systems Laboratory, Jožef Stefan Institute, Jamova cesta 39, Ljubljana SI-1000, Slovenia

ARTICLE INFO

Keywords:
Dovetail joints
Fretting fatigue
Slip accumulation
Contact behaviour
Stick-slip evolution
Crack initiation

ABSTRACT

Fretting refers to the small amplitude oscillatory relative motion between two contacting surfaces, which can occur due to various mechanical. When this relative motion occurs under cyclic loading conditions, it can cause surface damage and crack initiation through a process known as fretting fatigue. Fretting fatigue is a critical failure mechanism in many mechanical assemblies, particularly in dovetail joints of aircraft turbine engines. Accurate prediction of fretting fatigue lifetime relies on a thorough understanding of the evolution of contact behaviour. Existing studies have primarily focused on the spatial distribution of slip states under fixed loading conditions, with limited systematic analysis of the spatial-temporal evolution of slip–stick behaviour during cyclic loading. This study combines fretting fatigue experiments with finite element simulations to systematically characterise the contact behaviour of a flat-to-flat dovetail joint model under varying joint angles. By introducing the accumulated relative slip, the temporal and spatial evolution of slip and stick states are analysed. The study reveals, for the first time, three distinct stick-slip stages during loading cycles and their corresponding spatial distributions along the contact surface. Furthermore, within the framework of the modified Theory of Critical Distances (MTCD), the study further quantifies the independent influences of stick proportion and reverse slip magnitude on crack initiation lifetime. These results establish a direct link between contact behaviour evolution and fatigue damage, advancing the mechanistic understanding of fretting fatigue, and provide a theoretical basis and engineering reference for the design and reliability assessment of critical mechanical joint structures.

1. Introduction

Fretting refers to the small amplitude oscillatory relative motion between two contacting surfaces, which can occur due to various mechanical. When this relative motion occurs under cyclic loading conditions, it can cause surface damage and crack initiation through a process known as fretting fatigue. Fretting fatigue is a critical failure mechanism in many mechanical assemblies, particularly in dovetail joints of aircraft turbine engines [1–5]. This phenomenon is characterized by extremely small displacements and significant stress concentrations at the contact surface, which promote the initiation and rapid propagation of micro-cracks [6,7]. These cracks result in irreversible damage and significantly reduce the service life of structural components. In practical applications, many mechanical assemblies experience fretting fatigue during service, such as bearings, bolted joints, and gears [8]. Among these, one of the most critical and well-known cases is found in aircraft turbine engines. In such engines, blades and disks are typically connected through dovetail joints, where fretting fatigue at the contact interfaces can lead to crack initiation at the blade root, ultimately compromising engine safety and longevity [9,10]. As a result, fretting fatigue in dovetail joints has been identified by the U.S. Air Force as a high-risk issue during aircraft service life [11].

To better analyse the impact of fretting fatigue on component lifetime, researchers have proposed various theoretical approaches to predict the fatigue behaviour of materials, with the most main being the Continuum Damage Mechanics (CDM) and the Critical Plane (CP)

* Corresponding author.
** Corresponding author at: Soete Laboratory, Department of Electrical energy, metals, mechanical constructions and systems, Faculty of Engineering and Architecture, Ghent University, Belgium.
E-mail addresses: lhwang@tongji.edu.cn (L. Wang), Magd.abdelwahab@UGent.be (M. Abdel Wahab).

https://doi.org/10.1016/j.triboint.2025.111368
Received 4 June 2025; Received in revised form 7 October 2025; Accepted 30 October 2025
Available online 31 October 2025

theory. CDM, developed within a thermodynamic framework, focuses more on the evolution of microscopic damage and enables comprehensive modelling of the entire fatigue damage process [12–14]. While, CP theory identifies the most critical plane within the material where crack initiation is most likely to occur, making it well-suited for handling complex multiaxial stress states [15,16]. Since this study focuses on the prediction of crack initiation lifetime, the CP theory is adopted for its simplicity and efficiency. A detailed description of the CP theory is provided in Section 2.

The slip-stick behaviour at the contact interface plays a crucial role in the investigation of fretting fatigue mechanisms. It characterizes the relative motion between two contacting surfaces, which directly influences stress distribution, energy dissipation and crack initiation. A thorough understanding of contact behaviour is essential for the development of more accurate and reliable fatigue lifetime prediction models. Researchers often assess the distribution of stick and slip states by examining shear stress distribution under maximum load conditions [8,17,18]. Conner and Nicholas [19] attempted to analyse contact behaviour in a dovetail joint model with pads by evaluating shear stress at different loading stages. Their results indicated the presence of varying contact states throughout the loading process, although no definitive conclusions were drawn. Glodek and Talemi [2] proposed using the ratio of fretting fatigue stress, coefficient of friction and normal contact pressure as a key parameter for identifying stick or slip state. However, no quantitative explanation or clarification was provided. Mugadu et al. [20] developed a fretting fatigue model featuring a flat pad with rounded edges. By varying the ratio between the half-width of the flat portion of the indenter and the half-width of the contact area, they analysed the resulting contact pressure distributions and briefly examined the corresponding slip and stick zones under different loading conditions.

In previous studies on fretting fatigue, the concept of partial slip has been commonly used to describe the spatial distribution of slip and stick within the contact region at a given moment. However, it is often difficult to determine the temporal evolution of the contact state at a specific point, which may dynamically alternate between sticking and slipping. This time-dependent behaviour can be characterized as slip-stick. Although some studies have addressed either the spatial or temporal aspects of slip-stick phenomena, few have systematically investigated their coupled evolution across both dimensions during cyclic loading. In this study, a novel approach is proposed by introducing the accumulated relative slip as a metric to evaluate the temporal and spatial stick-slip evolution at the contact region. Furthermore, the relationship between slip-stick transitions and crack initiation is explored, providing theoretical insights to support more accurate fretting fatigue lifetime prediction.

2. Methodology

2.1. Critical plane theory

In the field of multiaxial fatigue research, the CP theory has been widely adopted as an effective approach for predicting fatigue lifetime. This theory posits that fatigue cracks tend to initiate on a specific plane oriented in such a way that it experiences the most severe damage [21,22]. This, so-called critical plane, is the surface where the fatigue damage reaches its maximum, and crack initiation is most likely to occur. To quantitatively evaluate the level of damage on the critical plane, various researchers have proposed different fatigue damage parameters within the framework of the CP theory. These parameters are designed to account for different loading conditions and fatigue regimes. Among the most used are the Findley Parameter (FP), the Fatemi–Socie Parameter (FS), and the Smith–Watson–Topper Parameter (SWT) [23,24]. Each of these damage models incorporates distinct physical quantities and assumptions to predict crack initiation under complex multiaxial stress states, making them suitable for different applications in fatigue analysis.

The FP parameter is one of the earliest fatigue damage criteria based on the CP theory. It considers the maximum shear stress as the primary driver for crack initiation while accounting for the auxiliary influence of normal stress [25]. By incorporating the maximum normal stress as a correction factor, a comprehensive fatigue criterion is established, making it suitable for lifetime prediction under high-cycle fatigue (HCF) conditions. The FP criterion effectively describes shear-dominated fatigue behaviour, particularly under complex tensile-shear combined loading.

The FS parameter is more applicable to Low-Cycle Fatigue (LCF) conditions. It uses the shear strain amplitude as the main control variable and incorporates the maximum normal tensile stress during the load cycle as a weighting factor to account for the embrittlement effect of tensile stress [26]. This makes the FS parameter particularly well-suited for scenarios involving significant plastic deformation.

The SWT parameter, proposed by Smith, Watson, and Topper, emphasizes the combined effect of the maximum principal stress and strain amplitude. It quantifies fatigue damage by the product of the maximum principal stress and the corresponding strain amplitude in the principal direction [18].In this study, the majority of fretting fatigue tests were conducted within the range of 10^4–10^5 cycles, corresponding to the transition region between LCF and HCF. This makes SWT especially appropriate, as it can capture the interaction between stress- and strain-driven damage mechanisms across this transitional fatigue regime.

Compared with the Findley Parameter (FP) and Fatemi–Socie (FS) parameter, which primarily emphasize shear strain and shear stress respectively, the SWT parameter provides a more balanced representation of the crack initiation process. Moreover, our previous investigations under similar contact geometries [27] have shown that both FS and FP criteria yield less accurate predictions of fatigue damage orientation, while SWT demonstrates better agreement with experimental results. Based on these considerations, the SWT criterion is adopted in the present work. It is also worth mentioning that friction heat is neglected in the adopted approach, which is a limitation and requires further improvement in future research. The basic expression for SWT is given by Eq. (1):

$$SWT = \sigma_{\max}\frac{\Delta\varepsilon}{2} = \frac{\sigma_f'^2}{E}(2N_i)^b + \sigma_f'\varepsilon_f'(2N_i)^{b+c} \tag{1}$$

where $\sigma_{\max}$ and $\Delta\varepsilon$ are the maximum normal stress and the maximum normal strain range. σ_f' is the fatigue strength coefficient (1460.16 MPa), E stands for Young's modulus, ε_f' is the fatigue ductility coefficient (0.33777), b and c are the exponents for fatigue strength and fatigue ductility(-0.10124 and −0.60152) [28].

2.2. Theory of critical distances (TCD)

In the analysis of contact fatigue, due to the relative motion between two contact surfaces, the stress distribution in the region of the contact surface is uneven, often exhibiting areas of high stress concentration, leading to a significant stress gradient. Relying solely on the maximum damage parameter for fatigue lifetime prediction may result in overly conservative estimates. The Critical Distance Theory (TCD) addresses this by introducing a 'critical distance' parameter, which averages the damage parameters in the stress-concentrated region within a defined distance, yielding an average damage parameter that better represents the overall material state [29–31]. In this study, considering the balance between computational time and accuracy, the Line Method (LM) is selected to average the damage parameters for fatigue lifetime prediction. LM averages the damage parameters of all nodes along the depth direction of the contact surface within the critical distance and uses this average as the representative damage parameter for the material's overall condition.

In calculating the critical distance, the MTCD method from the authors' previous research is adopted [27]. This method, based on the variable-TCD, considers both the maximum principal stress and its stress gradient. Under complex stress conditions, the maximum principal stress, as an extreme value, reflects the critical stress, while the stress gradient, as the rate of change, describes the variation in the stress distribution. Together, these two parameters provide a more comprehensive description of the stress distribution and offer a more reliable basis for fatigue lifetime prediction.

In finite element analysis, the stress gradient at each node can be calculated using a numerical difference approach, as shown in Eq. (2):

$$G = \frac{d_\sigma}{d_y} \approx \frac{\sigma_{i+1} - \sigma_i}{y_{i+1} - y_i} \quad (2)$$

where G represents the stress gradient, σ is the principal stress, and y is the depth. In this equation, σ_{i+1} and σ_i represent the principal stresses at adjacent nodes $i+1$ and i, while y_{i+1}- y_i indicates the distance between them. To improve prediction accuracy, this study incorporates both the maximum principal stress and the maximum stress gradient into the correction of the critical distance. Based on the initial critical distance L_0 obtained from the variable-TCD method, the modified critical distance L_c for TC4 is calculated using Eq. (3) [27]:

$$L_C = 1.477\sqrt{\frac{\sigma_{\max}}{G_{\max}} \times L_0} \quad (3)$$

where $\sigma_{\max}$ and G_{max} corresponding to the maximum principal stress and the maximum stress gradient, and L_0 is the initial critical distance obtained through the variable-TCD.

The MTCD method is implemented as follows: first, a finite element simulation of the dovetail joint model is conducted using ABAQUS to obtain the stress distribution in the contact region. Then, the principal stress distribution is extracted, and the maximum stress gradient is calculated using Eq. (2). Based on the initial critical distance L_0 obtained from the variable-TCD method, the final critical distance L_c is computed using Eq. (3). Simultaneously, Python is used for post-processing to obtain the distribution of the SWT damage parameter in the contact region. The LM is then applied to average the SWT damage parameter, yielding the mean damage value. Finally, Eq. (1) is used to calculate the crack initiation lifetime under the given loading condition. The detailed procedure can be referred to in the MTCD method flowchart shown in Fig. 1.

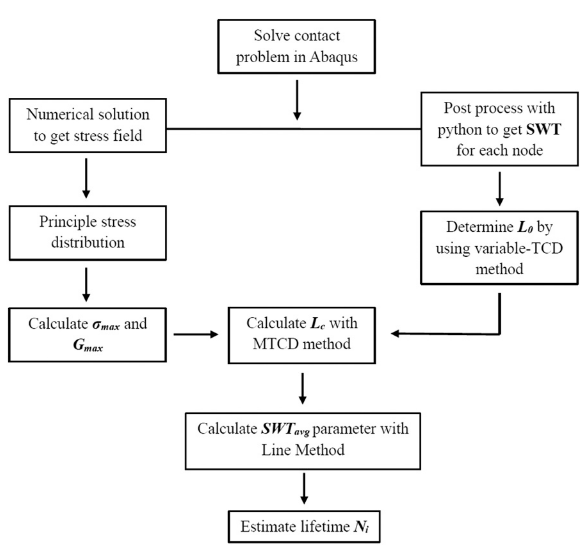

Fig. 1. Flowchart for the implementation of MTCD method [27].

3. Experimental validation

3.1. Experimental data

To investigate fretting fatigue behaviour at the blade-disk interface in aircraft turbine engines, a sub-scale dovetail specimen and corresponding fixture were designed in Ref. [28]. The specimen is made of TC4 titanium alloy, a typical α+β titanium alloy, with its material properties listed in Table 1.

The designed dovetail specimen has a thickness of 96 mm, which offers greater practical relevance than traditional thin-plate specimens. A symmetric dual-root configuration is employed, allowing two test results to be obtained from a single experiment. The fretting fatigue tests of the dovetail joint structure were conducted using a servo-hydraulic testing machine. The tests were performed under uniaxial cyclic loading conditions with a load ratio of 1/16. The contact between the dovetail slot and the tenon is of a flat-on-flat type, with a joint angle of 55°. The experimental equipment and the geometrical dimensions of the dovetail joint are shown on Fig. 2. The current study applies a single uniformly distributed load on the blade's upper surface, contrasting with conventional fretting fatigue tests where normal, tangential, and shear stresses are independently prescribed and measured. In our configuration, these stress components emerge naturally through contact interactions under the applied load, with their distributions determined computationally via finite element analysis rather than through experimental measurement.

The experimental results are listed in Table 2. Among the cases, T1, T3, and T5 correspond to the upper dovetail joint, while the others represent the lower dovetail joint. The measured lifetimes correspond to the total fatigue lifetime. The six experimental test results serve dual purposes: (1) calibrating and validating our fatigue lifetime prediction model through time-to-fracture data, and (2) verifying modelling accuracy by comparing predicted versus observed crack initiation locations and propagation angles, the details are shown in 4.3.

The applied stress σ is calculated from the concentrate cyclic force F using Eq. (4):

$$\sigma = \frac{F}{A} \quad (4)$$

where A is the area of the contact surface (621.6 mm^2) through which the load is actually transmitted.

3.2. Finite element analysis

In this study, a 2D Finite Element (FE) model was developed using ABAQUS to investigate the fretting fatigue behaviour. The FE model of the dovetail joint developed in this study is shown in Fig. 3. Considering the symmetry of the dovetail joint structure, only half of the geometry was modelled, and symmetric boundary conditions were applied along the central axis. The bottom surface of the fixture was fully constrained in both the x and y directions. A linear elastic constitutive model was used in the simulation, with CPE4 elements (four-node plane strain elements) employed for analysis. The contact interface between the dovetail slot and the dovetail tenon was defined as a contact pair. To improve the accuracy of stress distribution analysis and fatigue lifetime prediction, a local partitioning of the contact region was performed, and mesh refinement was applied to the lower surface beneath the contact

Table 1
The mechanical characteristics and physical properties of TC4 titanium alloy [28].

Young's modulus (GPa)	Yield strength (MPa)	Ultimate tensile strength (MPa)	Poisson ration	Density (kg/m3)
109	880	938	0.34	4400

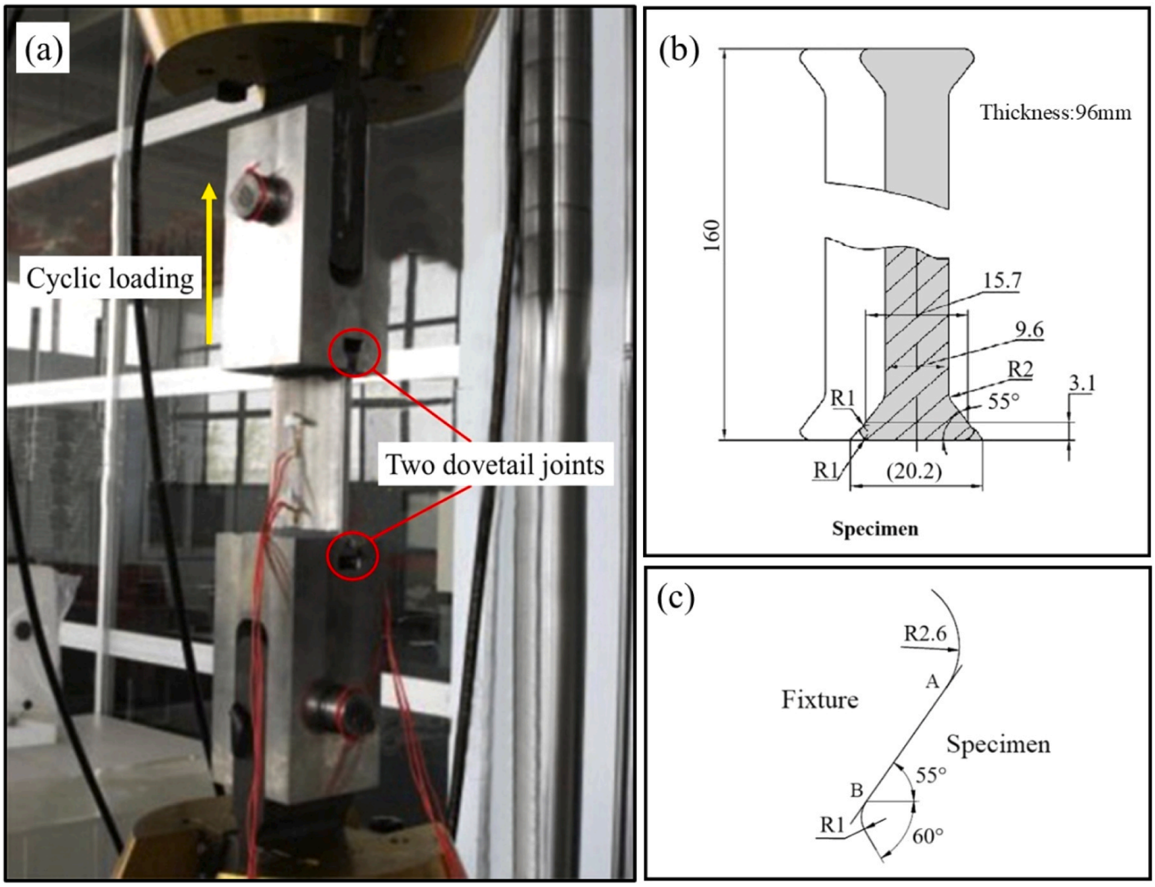

Fig. 2. Experimental setup and geometric details of the dovetail joint [28]: (a) overview of the experimental setup, (b) geometric dimensions of the specimen and (c) detailed dimensions of the contact surface.

Table 2
The fretting fatigue test results for the dovetail joint with pads model [28].

Test No.	F_{max} (kN)	F_{min} (kN)	σ_{max} (MPa)	σ_{min} (MPa)	N_f (cycles)
T1	161.7	10.11	175	10.94	101193
T2	161.7	10.11	175	10.94	74700
T3	191.7	11.94	208	13.00	44403
T4	191.7	11.94	208	13.00	62408
T5	210.7	13.17	228	14.25	42550
T6	210.7	13.17	228	14.25	39025

area over a length of 0.5 mm along the contact direction. Mesh sensitivity analysis has been well-established in prior studies [32]. Therefore, the element size of 0.002 mm was selected based on existing literature and the requirements of the MTCD approach to ensure accurate stress gradient resolution. The load is applied to the top of the specimen using a non-linear loading scheme, as shown in Fig. 3(c), where σ_{min} represents 1/16 of σ_{max}.

For the contact problem in dovetail joint structures, the commonly used algorithms are the Lagrange multiplier method and the penalty method. Both the penalty method and Lagrange multiplier method are theoretically viable for this contact simulation, though each presents distinct limitations. The Lagrange multiplier method [33], while providing exact constraint enforcement, suffers from three key drawbacks: (1) introduction of additional degrees of freedom increases computational cost, (2) numerical instability may occur during large sliding conditions, and (3) implementation complexity rises significantly for non-matching meshes. Conversely, the penalty method's primary limitations involve (1) inevitable elastic penetration at contact interfaces and (2) sensitivity to penalty stiffness parameter selection [34]. However, for flat-to-flat contact structures, convergence issues are often encountered. The penalty method, which allows for slight interpenetration, exhibits better adaptability and numerical stability in such cases. Therefore, the penalty method is adopted in this study, with the coefficient of friction set to 0.5. Contact segmentation method adopted in this analysis is segment-to-segment method. The FE model used in this study is an implicit model. The step type applied is Static, General, and the convergence tolerance is set to 0.5 %.

To better analyse the contact behaviour and crack initiation, the global coordinate system (x, y) was transferred to establish a local coordinate system (x', y'). The origin of this local system is set at the centre of the contact surface, with the x' - axis aligned along the contact interface and the y'-axis oriented perpendicular to it. Therefore, all location-related data presented hereafter are referenced to the local coordinate system. In this study, wear and oxidation effects are not included in the numerical model. This simplification is adopted to focus specifically on the mechanical role of slip in fretting fatigue crack initiation.

The MTCD method is employed to calculate crack initiation lifetime under different loading conditions based on the simulation results. In the authors' previous work, the MTCD approach demonstrated excellent applicability in predicting the fatigue lifetime of dovetail joints, with the smallest error observed in the T6 case only 0.6 % deviation from the experimental result, as shown in Fig. 4. As for the other data points, detailed explanations have already been provided in our earlier publications Ref. [27].

Therefore, the subsequent investigation of contact behaviour in various dovetail joint configurations is conducted based on this validated model. Since variations in the dovetail angle are expected to influence contact behaviour, this study examines the effect of joint angle

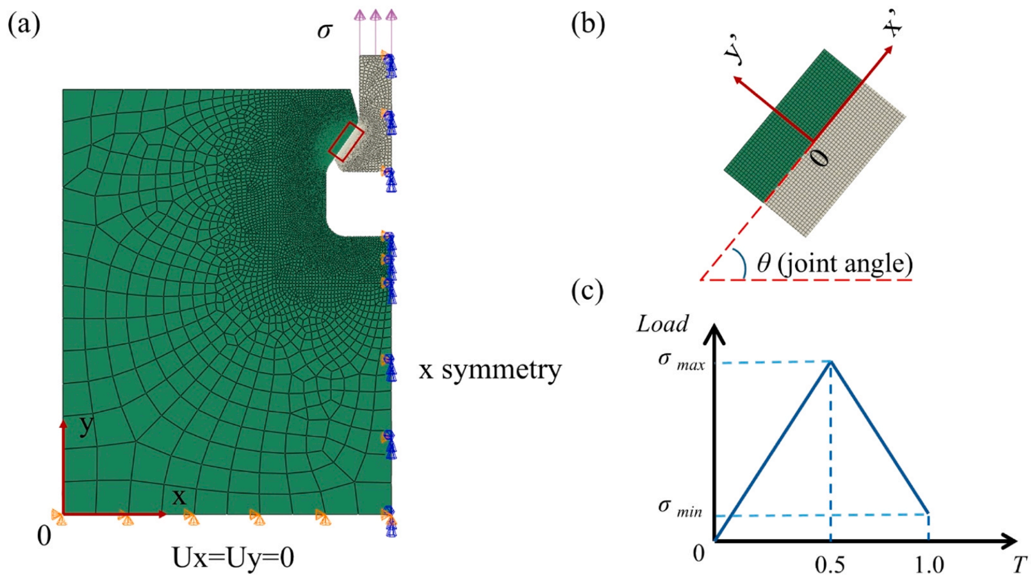

Fig. 3. The FE model for the dovetail joint model: (a) boundary and loading conditions, (b) enlarged view of the contact region and (c) load application.

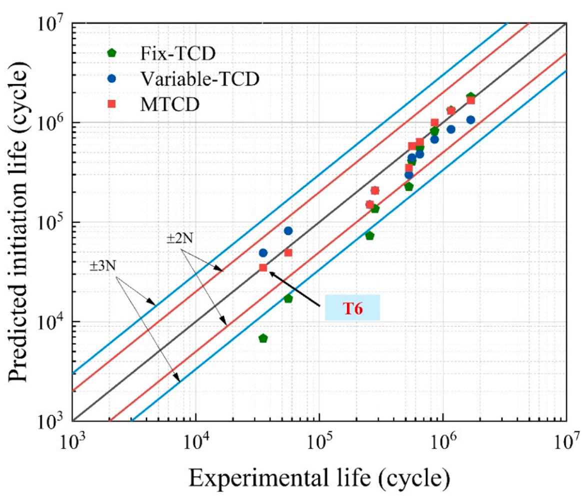

Fig. 4. Comparison of predicted and experimental lifetimes [27].

on slip characteristics and its subsequent impact on fatigue lifetime, while keeping all other parameters constant. The selected joint angles are 20°, 30°, 35°, 40°, 45°, 50°, 55°, 60°, and 70°, with 55° used as the validation test. An applied stress of 228 MPa is used in all tests.

4. Results and discussion

4.1. Spatiotemporal analysis of contact behaviours

In the study of fretting fatigue, existing literature often classifies contact behaviour on a regional basis, typically dividing the contact conditions into stick, slip, or stick-slip. The stick state refers to a state where the relative displacement at the contact point remains zero throughout the entire loading process, indicating that no sliding occurs at any time. In contrast, the slip state involves continuous relative sliding at the contact interface. The stick-slip state describes a situation in which the contact surface alternates between sticking and slipping over time, reflecting transitions between adhesion and sliding phases. However, for complex structures such as dovetail joints, there is still a lack of in-depth investigation into the specific evolution of contact behaviour during the fretting process. Most studies tend to describe the contact interface in general terms as being in a stick-slip zone, without fully acknowledging that fretting is inherently a dynamic phenomenon. In reality, fretting fatigue occurs across multiple positions on the contact surface and evolves continuously with cyclic loading. Therefore, a systematic analysis of the temporal and spatial evolution of contact behaviour is essential for revealing the underlying contact mechanisms driving fretting fatigue.

In ABAQUS, Contact Slip (CSLIP) is used to describe the accumulated relative slip at the contact interface, typically referring to the total tangential displacement between two contacting nodes. To better characterize the spatial and temporal evolution of fretting fatigue, this study analyses the contact behaviour of different nodes at various time points from both spatial and temporal perspectives. To better illustrate the contact behaviour at various points on the contact surface, Fig. 5 presents the variation of CSLIP at different positions during the loading cycle. To investigate contact behaviour at different positions along the contact surface during the fretting process, three representative points on the blade are selected: the lower edge (Point A), the middle (Point B), and the upper edge (Point C), as shown in Fig. 5(a). Fig. 5(b) presents the CSLIP evolution of these points over a full loading cycle. The time 0.5 corresponds to the maximum value of the cyclic load, while time 1 corresponds to the minimum load before transitioning into the next loading cycle.

Focusing on Point B, the cumulative slip increases continuously during the loading stage, indicating that slip occurs at this position. It means that point B is in a slip state during loading stage. However, as unloading begins, the cumulative slip remains constant for a period, which suggests that Point B enters a stick state. Toward the end of the unloading stage, the cumulative slip begins to increase in the opposite direction, revealing that Point B undergoes reverse slip during the unloading stage. For Point A, the CSLIP value remains zero during the early loading stage. Because it is initially outside the contact region. As the loading progresses, the normal pressure perpendicular to the contact interface increases, expanding the contact region and bringing Point A into contact with the disk. Once contact is established, Point A begins to slip together with other points in the contact region until the end of the loading phase. During unloading, its behaviour is similar to that of Point B, i.e. it first enters a stick state, followed by a reverse slip at the end of the unloading stage. However, since Point A joins the contact region later than Point B, its maximum cumulative slip is smaller. The contact behaviour of Point C is relatively straightforward to interpret. Initially, its cumulative slip increases are similar to that of Point B during the

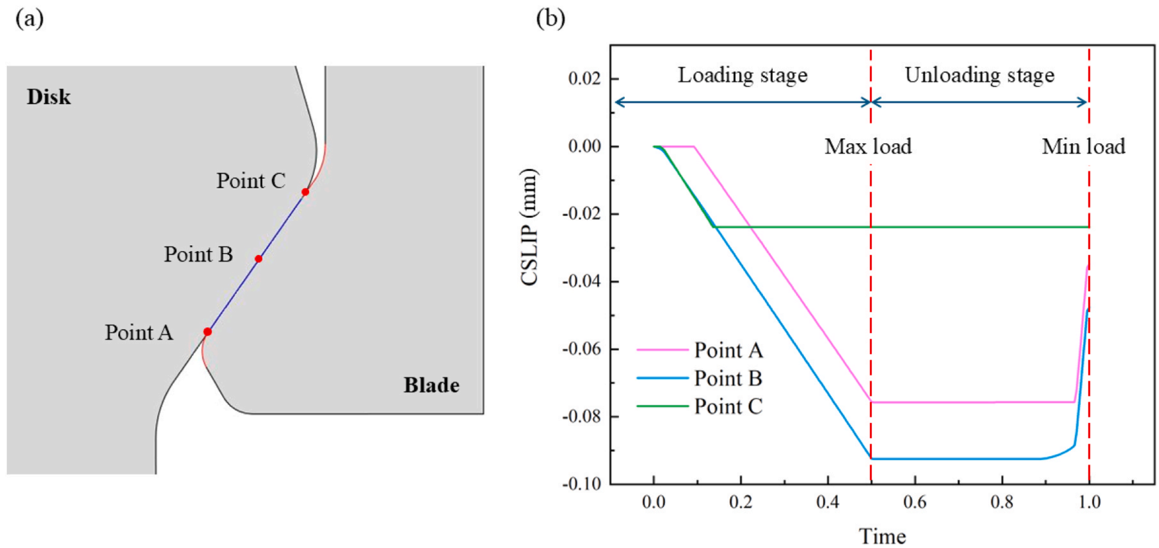

Fig. 5. Temporal evolution of relative slip at different positions within the contact surface: (a) illustration of selected positions and (b) variation of CSLIP values at different positions over one loading cycle.

loading stage, indicating that Point C is also involved in relative motion at the early loading stage. However, as the loading continues and displacement evolves, Point C gradually moves out of the contact region. Once it loses contact with the disk, no further relative slip occurs, and its CSLIP value remains constant from that moment onward.

To comprehensively investigate the contact behaviour at different positions across the contact interface, this study employs 3D surface plotting to visualize the spatiotemporal evolution of slip at various positions over time. By comparing dovetail joint structures with varying joint angles, the analysis reveals how contact behaviour evolves

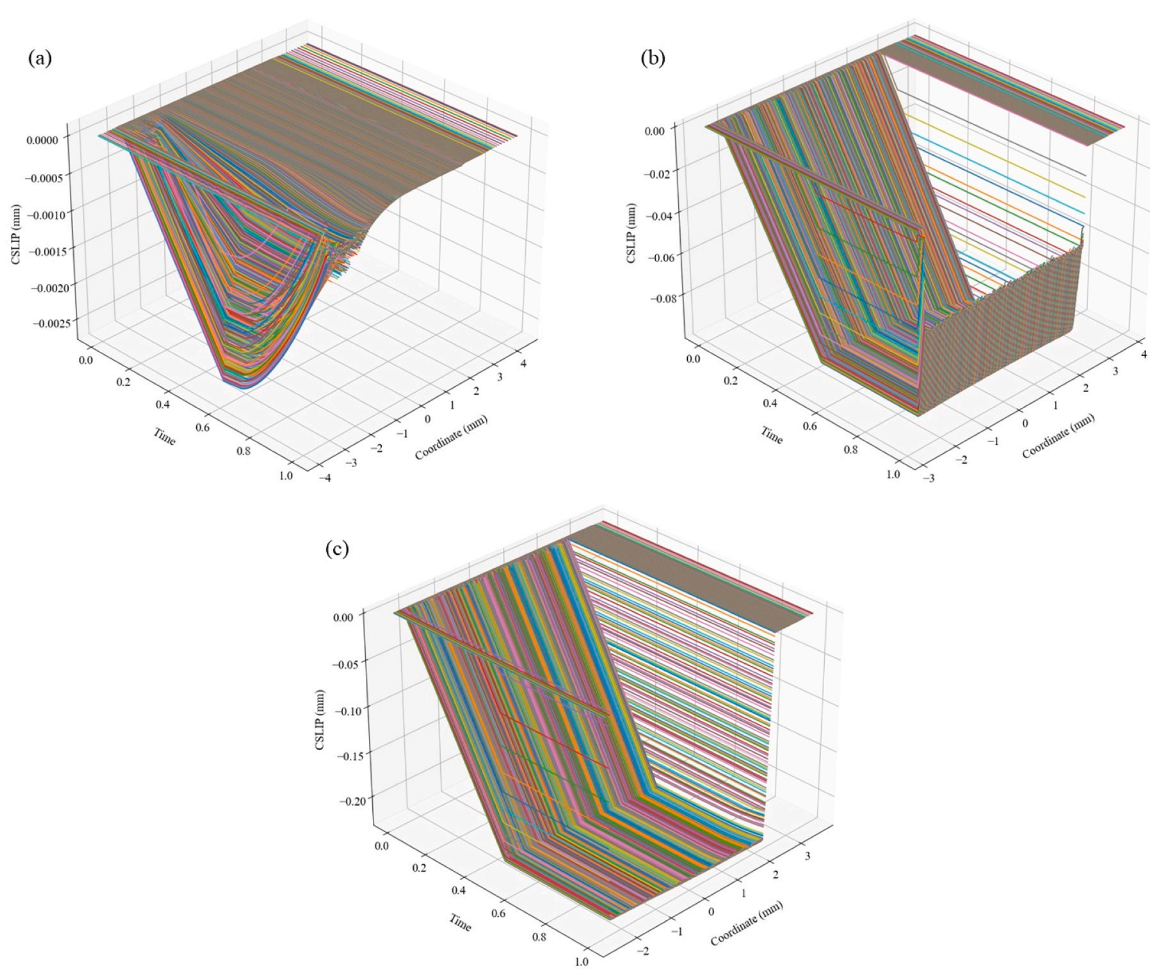

Fig. 6. Spatiotemporal evolution of contact behaviour in dovetail joint models with varying joint angles: (a) 20°, (b) 55° and (c) 70°.

differently in space and time depending on the joint geometry. The results are illustrated in Fig. 6.

Fig. 6(b) presents the contact behaviour of the dovetail joint model with a joint angle of 55°. Spatially, the contact interface can be categorized into three distinct regions: the lower edge, the central region, and the upper edge of the contact surface. The characteristics of these regions are consistent with the analysis discussed previously in Fig. 5. Specifically, points along the lower edge of the contact interface initially remain out of contact, then gradually enter the contact zone and undergo a sequence of slip, stick, and reverse slip during the loading cycle. However, the timing of entry into the slip-active region and the slip amplitude varies across different positions. For points near the upper edge of the contact region, the contact behaviour begins in phase with the central region, but these points eventually move out of the contact zone as the cycle progresses. Again, the timing of exit and the magnitude of slip differ depending on the position. In contrast, points located at the centre of the contact interface exhibit a uniform contact behaviour: all points undergo forward slip during the loading phase, followed by a stick phase and then reverse slip during unloading. The slip amplitude in this central region remains consistent across all positions.

Fig. 6(a) illustrates the contact behaviour of the dovetail joint model with a joint angle of 20°. A clear distinction is observed between the upper and lower regions of the contact interface. The upper portion of the contact region consistently exhibits a pronounced stick behaviour throughout both the loading and unloading stages. In contrast, the lower region shows a forward slip during the loading stage, followed by a brief stick phase, and then transitions into reverse slip during unloading stage. Although the amplitude of slip varies across different positions in the lower region, the maximum slip value remains limited to approximately 2.5 μm. Therefore, it can be concluded that the contact interface of the 20° dovetail joint largely maintains a full-stick condition under the given loading cycle.

Fig. 6(c) presents the contact behaviour of the dovetail joint model with a joint angle of 70°. Overall, the observed behaviour is consistent with that of the 55° model. However, several distinctions become evident as the joint angle increases. Notably, the points located near the lower edge and central region of the contact interface no longer exhibit a pronounced reverse slip during the unloading phase. In addition, the overall slip amplitude increases with the joint angle. For the 70° model, the maximum slip reaches approximately 0.23 mm, nearly twice that observed in the 55° model (0.099 mm). Furthermore, a clear increase in the number of points located at the upper edge of the contact region can be observed, indicating an expansion of the upper edge region.

4.2. *Comparative analysis for different joint angles*

The 3D visualizations presented earlier reveal significant spatial differences in contact behaviour across the contact region, while the central contact region exhibits a consistent slip evolution pattern across all models. To better interpret the variation in contact behaviour associated with different joint angles, a two-dimensional comparative analysis is performed by extracting the central point of the contact region from each dovetail joint model. The results are illustrated on Fig. 7.

The curves corresponding to the 20° and 30° models almost entirely overlap in the figure, indicating a full-stick condition throughout the loading cycle. Starting from a joint angle of 35°, all dovetail joint models exhibit a complete slip state during the loading stage, with the slip magnitude increasing progressively with angle. However, distinct differences emerge during the unloading stage. Specifically, the duration of the stick state and the magnitude of reverse slip vary with inclination. Especially, at 70°, the model shows almost no significant reverse slip during unloading stage, indicating a substantial reduction in interface recovery behaviour.

The results of the 20° and 30° models differ significantly from those observed at higher joint angles. To further elucidate the distinct behaviour exhibited by the 20° and 30° models, a simplified mechanical analysis of the dovetail joint structure is conducted, as shown in Fig. 8.

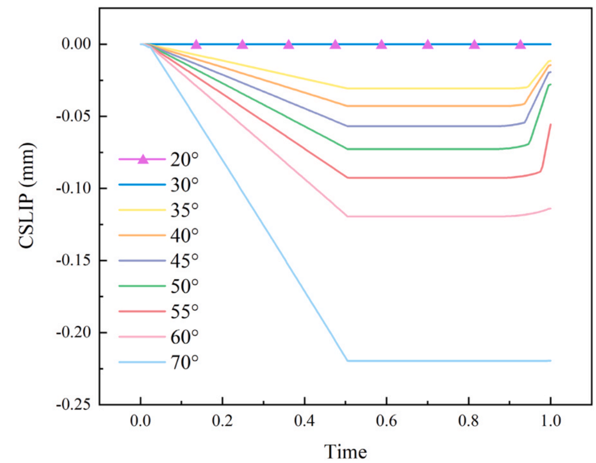

Fig. 7. CSLIP values of dovetail joint models with different joint angles.

The force analysis indicates that for a point to enter a slip state, the tangential force component must exceed the maximum static friction, which is defined as the product of the maximum static friction coefficient and the normal force, as described in Eq. (5):

$$F\sin\theta > f_s^{\max} = \mu_s F\cos\theta \tag{5}$$

where F is cyclic force, $f_s^{\max}$ is maximum static friction force, μ_s is the static coefficient of friction, and θ is joint angle. By further simplifying Eq. (5), the resulting expression is given in Eq. (6), in which the applied force is completely cancelled out:

$$\tan\theta > \mu_s \tag{6}$$

Therefore, the occurrence of slip at a given point is not governed by the applied force itself but solely by the joint angle. Specifically, when *tan* θ exceeds the maximum static friction coefficient of the contact interface, slip is possible. In contrast, when *tan* θ is smaller, the point cannot overcome static friction and will remain in a stick state regardless of the loading force applied. Based on the above analysis, the fully stick state observed in the 20° and 30° models can be attributed to the fact that *tan* θ does not exceed the maximum static friction coefficient. As a result, slip cannot be initiated in these models. When the joint angle reaches 35°, *tan* θ surpasses the critical threshold, enabling the onset of slip. From this angle onward, the loading phase exhibits a fully slipping condition.

To further investigate the variation in contact behaviour across models with joint angles ranging from 35° to 70°, two quantitative indicators are introduced: the proportion of stick state and the magnitude of reverse slip. The statistical results based on these parameters are presented in Fig. 9. Fig. 9(a) demonstrates that the proportion of stick state initially decreases with increasing angle, reaching a minimum at 50°, before subsequently rising, peaking at 70° with a value of 45.67 %.

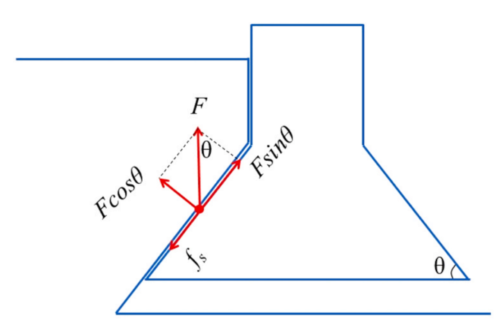

Fig. 8. Simplified force analysis of the dovetail joint structure.

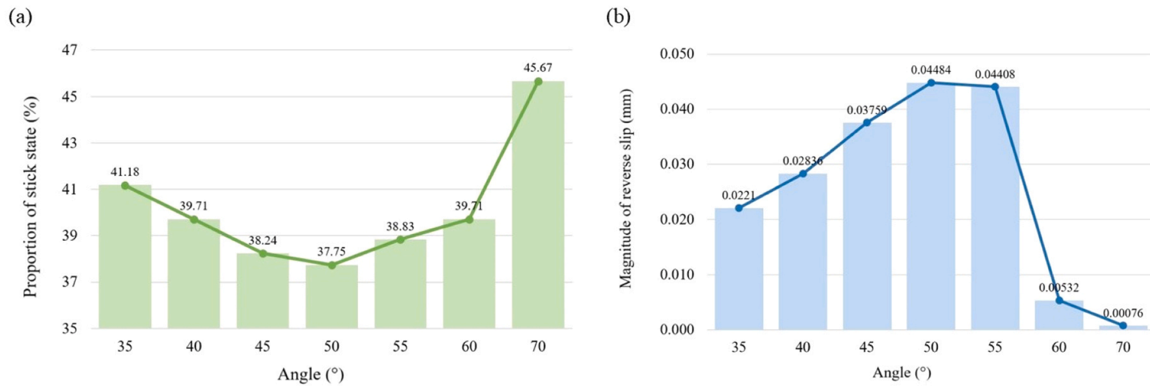

Fig. 9. Comparison of contact behaviour during the unloading stage in different dovetail joint angles: (a) proportion of stick state under different joint angles and (b) magnitude of reverse slip under different joint angles.

This trend indicates that, for moderate angles, the contact surface experiences more extensive sliding behaviour, while at lower and higher joint angles, the stick state tends to dominate for longer durations. Fig. 9 (b) reveals the evolution of reverse slip magnitude. From 35° to 50°, the reverse slip increases steadily, with a peak at 50° (0.04484 mm), indicating significant displacement in the unloading stage. However, a sharp decline is observed beyond 55°, with reverse slip nearly disappearing at 70°, reducing to just 0.00076 mm. At the same time, by comparing the trends of the proportion of stick state and the magnitude of reverse slip, it can be observed that at 50°, the stick proportion reaches its minimum while the reverse slip magnitude attains its maximum. However, this does not imply a direct inverse correlation between the two parameters. For instance, although the 45° model exhibits a lower proportion of stick state compared to the 55° model, its reverse slip magnitude is still smaller. This indicates that the two parameters are mutually independent and respond differently to variations in joint angle, each reflecting distinct aspects of the underlying contact mechanics.

Based on the above analysis, it can be concluded that in dovetail joint structures with excessively small angles, contact behaviour is completely suppressed, resulting in a fully stick state. However, as the angle increases, the slip mechanism does not exhibit a monotonic relationship with the joint angle. Especially, in the range of 45° to 55°, the reverse slip during the unloading stage is most pronounced, accompanied by the shortest duration of the stick state. In contrast, when the joint angle is either too small or too large, the contact behaviour is significantly diminished. This phenomenon highlights the critical role of geometric design in enhancing the mechanical performance of dovetail joints under cyclic loading conditions.

4.3. *Crack initiation analysis*

4.3.1. *Crack initiation position and angle*

The analysis of crack initiation holds significant importance in the study of fretting fatigue. This section focuses on investigating the influence of different dovetail joint angles on crack initiation behaviour during the fretting fatigue process. The SWT damage parameter is employed to predict the location of the most severe fatigue damage, which corresponds to the crack initiation site. To better illustrate the specific location of crack initiation, the ratio x'/a is used, where a represents the half-width of the contact area (the distance from the contact centre point to the contact edge), and x' denotes the distance from the contact centre point to the position of the maximum SWT value (the coordinate of the crack initiation point). The crack initiation positions for different angles are summarized and presented in Table 3.

From Table 3, it can be observed that as the joint angle increases, the half-width of the contact region (a) exhibits a slight decreasing, then increasing trend, reaching its minimum value of 2.5111 at 50°, indicating a temporary contraction of the contact length. In contrast, the crack initiation coordinate (x') consistently decreases with increasing joint angle, suggesting that the crack initiation point gradually shifts closer to the centre of the contact region. Moreover, the positive values of x' across all angles confirm that the crack always initiates on the upper edge of the contact region.

Table 3
Crack initiation positions at different dovetail joint angles.

Joint angle θ (°)	a (mm)	x' (mm)	x'/a
20	2.542	2.54	0.999
30	2.5341	2.5341	1.000
35	2.5222	2.5201	0.999
40	2.5153	2.5133	0.999
45	2.5139	2.5059	0.996
50	2.5111	2.4911	0.992
55	2.5123	2.4743	0.985
60	2.5124	2.4483	0.974
70	2.5216	2.3616	0.937

However, when considering the relative position expressed by the ratio x'/a, a different trend emerges. For joint angles between 20° and 45°, x'/a remains nearly constant and close to 1.000, indicating that the crack consistently initiates near the upper edge of the contact zone. Starting from 50°, this ratio begins to decrease progressively. At 70°, x'/a drops to 0.937, clearly demonstrating a shift of the crack initiation point toward the centre of the contact region. This trend suggests that at joint angles of 50° and above, the crack initiation location tends to move inward toward the centre of the contact region.

Among the commonly used damage parameters for predicting crack initiation angles (FP, FS, and SWT), the authors' previous research has demonstrated that the SWT parameter offers superior reliability in predicting crack initiation angles for dovetail joint models with flat-to-flat contact [27]. Therefore, the SWT parameter is adopted in this study to predict the crack initiation angles. Since the simulation directly provides the crack initiation angles relative to the global coordinate system (x, y), a transformation is required to obtain the angles relative to the contact surface. To clarify the relationship between the predicted crack angles and the contact surface, the simulation results are converted accordingly. The transformation method is illustrated in Fig. 10,

As shown in Fig. 11, the red line represents the predicted crack initiation angle, which is in good agreement with the experimental results, confirming the reliability and accuracy of the SWT method. Although there is some debate regarding the appropriate definition of crack initiation length (50–100 μm), in this case it is clearly observed that the crack angle remains nearly constant over a length of approximately 2 mm. Therefore, the angle can be reasonably regarded as the crack initiation angle. Based on this validated test, further analyses were conducted to investigate the influence of dovetail geometry on the crack initiation angle, with the results listed in Table 4.

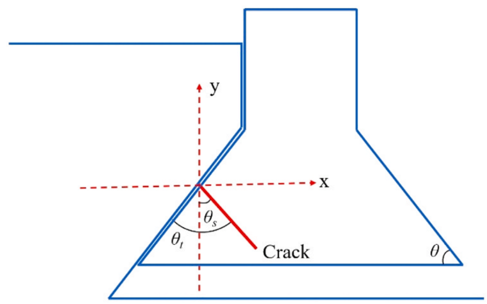

Fig. 10. Illustration of the angle transformation method.

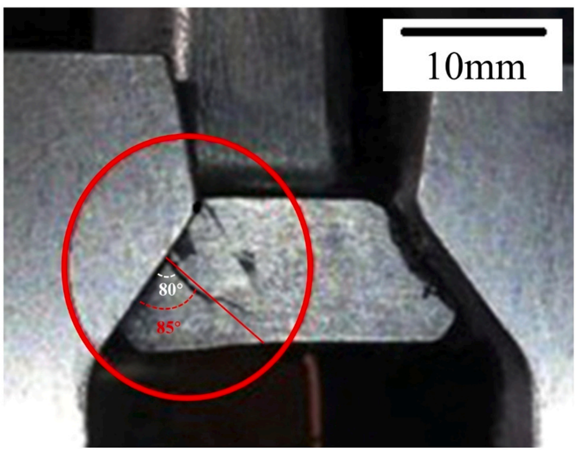

Fig. 11. Comparison of predicted and experimental initiation angle.

Table 4
Crack initiation angles at different dovetail joint angles.

Joint angle θ (°)	Simulation angle θ_s (°)	Transformed angle θ_t (°)
20	19	89
30	29	89
35	34	89
40	39	89
45	43	88
50	46	86
55	50	85
60	55	85
70	63	83

Through analysis, it is evident that when the dovetail joint angle ranges from 20° to 40°, the crack initiation angle relative to the contact surface remains nearly unchanged, staying almost perpendicular to the surface. Starting from 45°, as the joint angle increases, the crack initiation angle begins to decrease slightly, indicating a minor deflection of the crack path toward the contact surface. Given that crack initiation consistently occurs near the upper edge of the contact region, this suggests that increasing the joint angle causes the crack direction to shift slightly toward the centre of the contact region.

In summary, as the dovetail joint angle increases, there is no significant change in either the crack initiation position or angle within the range of 20° to 40°. However, beyond 45°, both the crack initiation position gradually shifts toward the centre of the contact region, and the crack initiation angle exhibits a noticeable deflection toward the same direction.

4.3.2. *Crack initiation lifetime*

The effect of dovetail joint angle on fatigue lifetime is investigated through its impact on contact mechanics. Crack initiation lifetime is evaluated for various angles using the MTCD method [27]. In addition, the correlation between contact behaviour and fatigue lifetime is explored based on the observed contact mechanisms across different angles. All the results are presented in Table 5.

It is first evident that the 20° and 30° models exhibit full stick state and correspondingly show the shortest initiation lifetime among all cases, indicating that sticking has a negative effect on fatigue lifetime. Although the 70° model also maintains stick state during the unloading stage, it still demonstrates a longer initiation lifetime than the 20° and 30° models due to the presence of slip during loading stage. Interestingly, the influence of reverse slip shows the opposite trend, i.e. given similar proportion of stick state, a larger reverse slip magnitude correlates with a longer initiation lifetime (e.g., 40° vs. 60°), suggesting a positive contribution of reverse slip to fatigue lifetime.

As previously discussed, the proportion of the stick state and the magnitude of reverse slip are two independent variables, and the fatigue lifetime of the dovetail joint structure is jointly influenced by both. To better show their respective impacts on crack initiation lifetime, a comparative analysis was conducted on dovetail joint models with joint angles ranging from 35° to 70°, excluding cases exhibiting full stick state. To more clearly illustrate the variation trends, the crack initiation lifetime, proportion of the stick state, and magnitude of reverse slip were evaluated and compared. The results obtained in Table 5 were normalized, focusing on the relative trends rather than absolute values. The comparative results are presented in Fig. 12.

Analysis reveals that the overall trend of crack initiation lifetime closely aligns with the magnitude of reverse slip, suggesting that reverse slip magnitude exerts a more pronounced influence on fatigue lifetime. When reverse slip magnitudes are similar (e.g., 50° vs. 50°), the proportion of the stick state also shows a measurable impact on crack initiation lifetime. Regardless of which factor dominates, both variables reach their extreme values at a joint angle of 50°, where the crack initiation lifetime is also the highest. This leads to a clear conclusion: shorter stick durations and greater reverse slip magnitudes are both beneficial for extending the crack initiation lifetime of dovetail joint structures.

5. Conclusions

This study is based on fretting fatigue experiments and FE simulations of a flat-to-flat contact dovetail joint model, providing a systematic analysis of its contact behaviour. Unlike previous studies that primarily determined stick or slip states based on the shear stress distribution under maximum load, this work is the first to investigate slip evolution from both temporal and spatial perspectives. The contact behaviour under varying joint angles was analysed in detail, and its influence on crack initiation lifetime was further explored, the following conclusions are drawn:

1. Contact behaviours varies with different loading stages. The contact behaviour mainly includes three types: forward slip during loading

Table 5
Contact behaviour and crack initiation lifetime at different dovetail joint angles.

Joint angle (°)	Proportion of stick state (%)	Magnitude of reverse slip (mm)	Initiation lifetime (cycle)
20	100.00	0.00000	15140
30	100.00	0.00000	16150
35	41.18	0.02210	20524
40	39.71	0.02836	24971
45	38.24	0.03759	29409
50	37.75	0.04484	40657
55	38.83	0.04408	34901
60	39.71	0.00532	21224
70	45.67	0.00076	19765

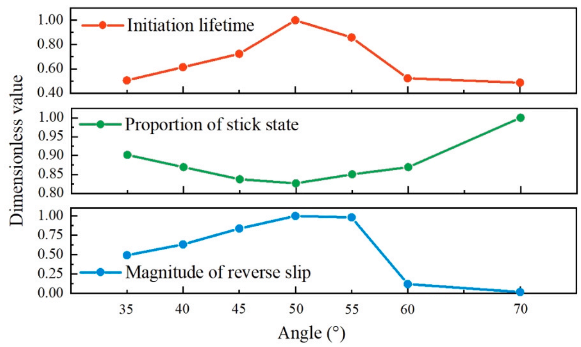

Fig. 12. Comparison of contact behaviour and initiation lifetime in different dovetail joint models.

stage, stick during unloading stage, and reverse slip at the end of unloading stage.

2. Spatially, most of the contact region shows a similar slip evolution trend. The upper edge experiences early slip and then moves away from contact surface, while the lower edge gradually enters the contact region and evolves with the rest points of the contact region.
3. Whether slip occurs during the loading stage depends only on the joint angle and is independent of the load magnitude. If the condition $\tan\theta < \mu_s$ is satisfied, the model remains in a full stick state and slip will not occur.
4. When the joint angle is between 20° and 45°, both the crack initiation position and angle remain unchanged, with cracks initiating at the upper edge of the contact region at an angle of approximately 89°. From 50° onward, both the initiation position and angle shift progressively toward the centre of the contact region.
5. The crack initiation lifetime is jointly controlled by two independent physical parameters: the proportion of the stick state and the reverse slip amplitude. The study reveals that the duration of the stick state is inversely proportional to the crack initiation lifetime, while the reverse slip amplitude shows a positive correlation with the lifetime. These findings provide valuable physical insights for developing more accurate lifetime prediction methods and establish a solid theoretical foundation for subsequent physics-based criteria for crack initiation lifetime.

6. Future work

In future work, the authors will focus on developing a refined criterion for predicting crack initiation lifetime in fretting fatigue, based on a combined analysis of local stress distribution, stick-slip behaviour, and cumulative frictional work. This approach aims to move beyond traditional stress-based methods by incorporating the temporal and spatial evolution of slip zones together with the total energy dissipated at the contact interface during cyclic loading. Frictional work, as a physically grounded cumulative quantity, may offer improved predictive capability and better generality, particularly for application to more realistic 3D dovetail configurations. In this context, the use of a Lagrange contact enforcement method will be considered, together with strategies to retain high computational efficiency while relying on a more robust and reliable contact algorithm. Furthermore, this framework has the potential to be adapted for other types of joints involving fretting-prone interfaces.

7. Limitations of the current study

Wear and oxidation are known to influence fretting fatigue behaviour through multiple mechanisms. Wear can modify the contact geometry and reduce stress concentration at the contact edge, which may delay or suppress crack initiation under certain conditions. However, under higher displacement amplitudes, increased wear can also lead to material removal and surface damage that promote fatigue crack formation. Oxidation can either form protective tribolayers that reduce damage or introduce brittle surface films that facilitate crack initiation, depending on temperature and environment. Although not included in the current model, these effects are important and will be considered in future extensions. Meanwhile, the crack initiation angles and fatigue lifetimes for different dovetail geometry angles have not been experimentally validated, except for the 55° test.

Statement of novelty

Unlike previous studies that primarily assessed slip-stick states based on static shear stress distributions, this work presents the first comprehensive investigation into their temporal and spatial evolution under cyclic loading in dovetail joints. Through combined experiments and simulations on a flat-to-flat contact model, three key contact stages are identified and linked to crack initiation mechanisms. Notably, the study quantifies the independent influence of stick proportion and reverse slip magnitude on fatigue lifetime, offering a new understanding of how joint geometry governs contact dynamics. This novel approach provides deeper mechanistic insight and enhances the predictive accuracy of fretting fatigue lifetime models for critical structural applications.

CRediT authorship contribution statement

Qiqi Xiao: Writing – original draft, Methodology, Investigation, Conceptualization. **Gang Chen:** Writing – review & editing. **Lihua Wang:** Writing – review & editing, Supervision. **Can Wang:** Software, Investigation. **Yuxuan Wu:** Investigation. **Magd Abdel Wahab:** Writing – review & editing, Supervision, Investigation, Conceptualization.

Declaration of Competing Interest

The authors declare that they have no known competing financial interests or personal relationships that could have appeared to influence the work reported in this paper.

Acknowledgment

This work is supported by the National Natural Science Foundation of China (Project no. 12272270) and the Shanghai Pilot Program for Basic Research. The authors acknowledge the support of the financial support of the grants from the China Scholarship Council (202507650026).

Data availability

Data will be made available on request.

References

[1] Yang Q, Zhou W, Gai P, Zhang X, Fu X, Chen G, et al. Investigation on the fretting fatigue behaviors of Ti-6Al-4V dovetail joint specimens treated with shot-peening. Wear 2017;372-373:81–90.
[2] Glodek G, Talemi R. An applied approach for estimating fretting fatigue lifetime of dovetail joints using coupon scale test data. Theor Appl Fract Mech 2022;121:103455.
[3] Wang Z, Chen T, Gong J, Zheng Y, Niu F, Wang Z, et al. Improvement in fretting fatigue life of GH4169 dovetail joint component by bonded solid lubricant coating at 500 ℃. Tribology Int 2024;193:109415.
[4] Waterhouse RB. Fretting fatigue. Int Mater Rev 1992;37(1):77–98.
[5] Hills DA, Nowell D. Introduction. In: Hills DA, Nowell D, editors. Mechanics of Fretting Fatique. Dordrecht: Springer Netherlands; 1994. p. 1–7.
[6] Zou L, Zeng D, Zhang Y, Lu L, Zhao H, Xu T, et al. A coupled wear and crack initiation-propagation methodology for fretting fatigue life assessment in press-fitted axles. Int J Fatigue 2022;159:106817.
[7] Rangel D, Erena D, Vázquez J, Araújo JA. Prediction of initiation and total life in fretting fatigue considering kinked cracks. Theor Appl Fract Mech 2022;119:103345.

[8] Croccolo D, De Agostinis M, Fini S, Olmi G, Robusto F, Scapecchi C. Fretting fatigue in mechanical joints: a literature review. Lubricants 2022.

[9] Lee B-W, Suh J, Lee H, Kim T-g. Investigations on fretting fatigue in aircraft engine compressor blade. Eng Fail Anal 2011;18(7):1900–8.

[10] Zhang R, Meng X, Sun K, Li Q, Zhao F. An investigation of high and room temperature fretting fatigue of DD6-FGH96 dovetail joint in aero-engine: Experimental and numerical analysis. Int J Fatigue 2022;154:106537.

[11] Chan KS, Enright MP, Moody JP, Golden PJ, Chandra R, Pentz AC. Residual stress profiles for mitigating fretting fatigue in gas turbine engine disks. Int J Fatigue 2010;32(5):815–23.

[12] Xu Y, Yuan F, Lin X, Zhang H. Numerical investigation to the effect of wear on fretting fatigue life using CDM and fracture mechanics. Eng Fract Mech 2024;306:110261.

[13] Shen F, Ke L-L, Zhou K. A debris layer evolution-based model for predicting both fretting wear and fretting fatigue lifetime. Int J Fatigue 2021;142:105928.

[14] Sun D, Huo J, Chen H, Dong Z, Ren R. Experimental study of fretting fatigue in dovetail assembly considering temperature effect based on damage mechanics method. Eng Fail Anal 2022;131:105812.

[15] Sunde SL, Berto F, Haugen B. Predicting fretting fatigue in engineering design. Int J Fatigue 2018;117:314–26.

[16] Salehi E, Polycarpou Andreas A. Fretting Fatigue Life Model Under Combined Loading. Fatigue Fract Eng Mater Struct 2025;48(1):16–30.

[17] Rajasekaran R, Nowell D. Fretting fatigue in dovetail blade roots: experiment and analysis. Tribology Int 2006;39(10):1277–85.

[18] Wang C, Li C, Ling Y, Wahab MAbdel. Investigation on fretting fatigue crack initiation in heterogenous materials using a hybrid of multiscale homogenization and direct numerical simulation. Tribology Int 2022;169:107470.

[19] Conner BP, Nicholas T. Using a Dovetail fixture to study fretting fatigue and fretting palliatives. J Eng Mater Technol 2003;128(2):133–41.

[20] Mugadu A, Hills DA, Nowell D. Modifications to a fretting-fatigue testing apparatus based upon an analysis of contact stresses at complete and nearly complete contacts. Wear 2002;252(5):475–83.

[21] Wang C, Fan K, Zhao Q, Wahab MAbdel. Effect of shot peening parameters on fretting fatigue lifetime. Tribology Int 2024;193:109311.

[22] Wang C, Wang D, Wahab MAbdel. Fretting fatigue crack initiation behaviour in heterogeneous materials under out-of-phase loading. Tribology Int 2022;171:107571.

[23] Shu Y, Yang G, Liu Z, Hu W. A comparative study of several life prediction models based on the critical plane approach for fretting fatigue crack initiation. Fatigue Fract Eng Mater Struct 2024;47(5):1495–513.

[24] Wang S, Yue T, Wang D, Abdel Wahab M. Effect of wear debris on fretting fatigue crack initiation. Friction 2022;10(6):927–43.

[25] Bhatti NA, Abdel Wahab M. A numerical investigation on critical plane orientation and initiation lifetimes in fretting fatigue under out of phase loading conditions. Tribology Int 2017;115:307–18.

[26] Díez Molina N, Vanegas Useche LV, Mesa CA, Wang C, Wang L, Wahab MAbdel. Fretting fatigue crack nucleation analysis under a variable coefficient of friction. Tribology Int 2024;194:109558.

[27] Xiao Q, Wang C, Ahmed B, Wang D, Cai Z, Wang L, et al. Prediction of fretting fatigue lifetime of dovetail joints using a modified theory of critical distances. Tribology Int 2025;209:110728.

[28] Hu C, Wei D, Wang Y, Shi L. Experimental and numerical study of fretting fatigue in dovetail assembly using a total life prediction model. Eng Fract Mech 2019;205:301–18.

[29] Taylor D. The theory of critical distances. Eng Fract Mech 2008;75(7):1696–705.

[30] Taylor D, Barrett N. G. Lucano, Some new methods for predicting fatigue in welded joints. Int J Fatigue 2002;24(5):509–18.

[31] Susmel L, Taylor D. Two methods for predicting the multiaxial fatigue limits of sharp notches. Fatigue Fract Eng Mater Struct 2003;26(9):821–33.

[32] Sun S, Li L, Yue Z, Yang W, He K, Li S. Fretting fatigue failure behavior of Nickel-based single crystal superalloy dovetail specimen in contact with powder metallurgy pads at high temperature. Tribology Int 2020;142:105986.

[33] Doca T, Andrade Pires FM. Finite element modeling of wear using the dissipated energy method coupled with a dual mortar contact formulation. Comput Struct 2017;191:62–79.

[34] Doca T, Andrade Pires FM, Cesar de Sa JMA. A frictional mortar contact approach for the analysis of large inelastic deformation problems. Int J Solids Struct 2014;51(9):1697–715.